JOURNAL OF GEOPHYSICAL RESEARCH, VOL. 103, NO. B3, PAGES 5269-5286, MARCH 10, 1998

Geomagnetic polarity reversal model of deep-tow profiles from the Pacific Jurassic Quiet Zone

William W. Sager,[1,2] Chester J. Weiss,[2] Maurice A. Tivey,[3] and H. Paul Johnson[4]

Abstract. The Jurassic magnetic "Quiet Zone" (JQZ) contains magnetic lineations, but their low amplitudes make correlation and interpretation difficult. Part of the problem is the separation of source and sensor for old, deep ocean crust. We increased anomaly amplitudes by collecting magnetic data along two deep-tow profiles over western Pacific JQZ lineations. A magnetic polarity reversal timescale was constructed by matching deep-tow anomalies with a simple, rectangular block magnetization model for oceanic crust. The polarity sequence covers ~11 m.y. (156-167.5 Ma) and contains 88 pre-M29 polarity chrons extending to Chron M41. A limitation of this model is its poor representation of the oldest anomalies upward continued to sea level. On deep-tow profiles these anomalies have both long- and short-wavelength components, but only the latter are easily modeled on a datum close to the source. An alternative polarity model was constructed to match the anomalies upward continued to sea level. This model retains only 44% of the deep-tow model polarity chrons because of short-wavelength attenuation by upward continuation. Because of the inferred periods and magnetization contrasts, we think many of the short-wavelength anomalies represent paleofield intensity fluctuations. In contrast, polarity reversals have been documented by prior magnetostratigraphic work for the younger part of the timescale covered by our model. Thus our data may show a transition from a geomagnetic field behavior dominated by intensity fluctuations to one dominated by reversals.

1. Introduction

Linear magnetic anomaly "stripes" are characteristic features of oceanic lithosphere that result from geomagnetic reversals recorded by the process of ocean crust formation. They exist because ocean crustal rocks are emplaced in a narrow, linear zone parallel to the mid-ocean ridge crest, crustal rocks preserve a remanent magnetization parallel to the ambient field at the time of formation, and the geomagnetic field has repeatedly changed polarity [*Vine and Matthews*, 1963]. Magnetic lineation studies have been carried out for many reasons, one of the more significant being that they constitute a continuous record of geomagnetic polarity epochs, and therefore, they are the foundation of much of the geomagnetic polarity timescale (GPTS). The basic approach in deriving a GPTS is to deduce a polarity time series using a simple alternating polarity block model of the upper ocean crust and to interpolate or extrapolate the dates for block boundaries using age calibration points [e.g., *Heirtzler et al.*, 1968; *Larson and Hilde*, 1975; *LaBrecque et al.*, 1977; *Cande and Kent*, 1992a; 1995].

Although magnetic lineations have been mapped throughout the world's oceans, they are not generally identified over seafloor of mid-Cretaceous or Middle to Late Jurassic age. The younger of these two gaps is termed the "Cretaceous Quiet Zone" and corresponds to a period of ~37 m.y. (83.5-120.4 Ma [*Gradstein et al.*, 1994]) when the geomagnetic field was demonstrably in a nearly constant normal polarity state [*Helsley and Steiner*, 1969] except perhaps for a few brief reversed intervals (see review by *Ogg* [1995]). The origin of the Jurassic "Quiet Zone" (JQZ) appears different. From land magnetostratigraphic data, it appears to be a period containing many geomagnetic field reversals [*Steiner and Ogg*, 1988; *Ogg*, 1995], but the resulting marine magnetic lineations are difficult to detect and correlate because of their low amplitudes. Indeed, several studies have shown an envelope of decreasing anomaly intensity going back into the Jurassic, with one explanation being a systematic reduction in field intensity going backward in time [e.g., *Hayes and Rabinowitz*, 1975; *Cande et al.*, 1978].

Initial studies of Jurassic crust suggested the JQZ was a period of constant normal [*Heirtzler and Hayes*, 1967; *Burek*, 1970; *Larson and Pitman*, 1972; *Larson and Hilde*, 1975; *Hayes and Rabinowitz*, 1975] or reversed polarity [*Taylor and Greenewalt*, 1976], but later magnetic anomaly studies systematically pushed the end of the JQZ backwards in time from Chron M22 to Chron M38 [*Larson and Hilde*, 1975; *Cande et al.*, 1978; *Handschumacher et al.*, 1988]. Polarity chrons back to M25 have been correlated in all the major ocean basins, whereas M26-M29 have only been positively identified over lithosphere created by rapid spreading in the Pacific (M26-M29) [*Cande et al.*, 1978] and eastern Indian oceans (M26) [*Sager et al.*, 1992]. Older lineations have been identified only in the Japanese lineation group at two locations in the western Pacific [*Handschumacher et al.*, 1988; *Nakanishi et al.*, 1992].

Handschumacher et al. [1988] identified pre-M29 lineations on eight closely spaced, low-altitude aeromagnetic profiles over the Pigafetta Basin, located east of the northern Mariana

[1]Department of Oceanography, Texas A&M University, College Station.
[2]Also at Department of Geology and Geophysics, Texas A&M University, College Station.
[3]Department of Geology and Geophysics, Woods Hole Oceanographic Institution, Woods Hole, Massachusetts.
[4]School of Oceanography, University of Washington, Seattle.

Paper number 97JB03404.
0148-0227/98/97JB-03404$09.00

Trench in the western Pacific Ocean (Figure 1). Correlation of these low-amplitude anomalies was possible, in part, because the high speed of the aircraft made it easier to separate the subtle magnetic lineations from geomagnetic noise, such as diurnal variations. Similar lineations were recognized on aeromagnetic and ship profiles from the East Mariana Basin, ~650 km south of the Pigafetta Basin, and identified back to M33 [*Handschumacher et al.*, 1988; *Nakanishi et al.*, 1992]. Anomalies at this location are more difficult to correlate, perhaps owing to effects of the widespread mid-Cretaceous volcanics, which were cored at nearby Ocean Drilling Program Site 800 [*Lancelot et al.*, 1990] and possibly because of a spreading ridge jump (R. L. Larson, personal communication, 1995).

Lineated anomalies have been found over lithosphere of similar age along the North Atlantic Ocean margins, but they have not been positively identified or correlated to Pacific anomalies because slow spreading rates and thick continental margin sedimentary deposits make their identification more difficult. Lineations in locations and orientations consistent with pre-M25 seafloor spreading anomalies have been recognized in the northwest Atlantic off the Nova Scotia margin [*Barrett and Keen*, 1976] and in the eastern Atlantic west of the Moroccan margin (H. Roeser et al., in preparation, 1997). These anomalies imply that the pre-M25 lineations are global geomagnetic features. Magnetostratigraphic data support this view with several studies reporting magnetic reversals within Middle to Late Jurassic sediments, implying

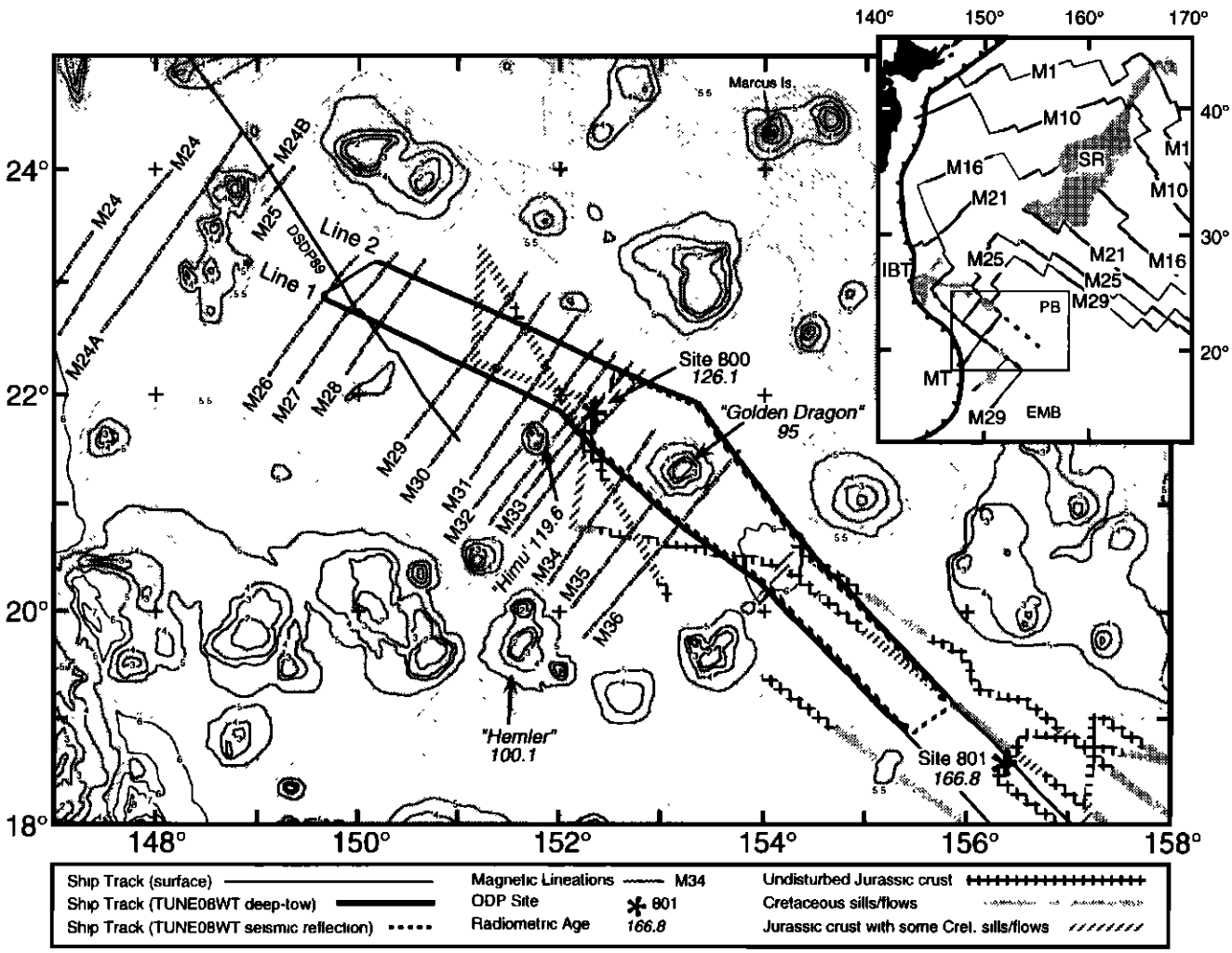

Figure 1. Location of study area and bathymetry, magnetic lineations, and ship tracks. Bathymetry contours at 1 km intervals; stipple shows region above 5.5 km depth [*Brenner and Angell*, 1992]. Shaded dashed lines oriented NE are magnetic lineations identified by *Handschumacher et al.* [1988]; note M29 and older lineations have been renumbered to be consistent with the M29 identification of *Cande et al.*, [1978] as noted in the text. Heavy solid lines denote deep-tow magnetic tracklines of R/V *Thomas Washington* cruise TUNE08WT, whereas lighter solid lines show the Leg 89 track of D/V *Glomar Challenger* used to connect the deep-tow-identified lineations with younger lineations. Stars mark the locations of Ocean Drilling Program (ODP) Sites 800 and 801 [*Lancelot et al.*, 1990] and numbers in italics give basalt core dates [*Pringle*, 1992]. Dated seamounts are labeled with names and radiometric dates in italics [*Ozima et al.*, 1983; *Smith et al.*, 1989]. The heavy line with variable patterns shows multichannel seismic reflection tracks used to characterize acoustic basement and interpret which areas were affected by mid-Cretaceous volcanism [*Abrams et al.*, 1993]. The inset shows the regional location of the study area (small box). Heavy lines show selected magnetic isochrons [*Nakanishi et al.*, 1989]. The heavy line with teeth represents western Pacific trenches (MT, Mariana Trench; IBT, Izu-Bonin Trench). The islands of Japan are shown in black silhouette. Stipple signifies large bathymetric features above 5 km depth (SR, Shatsky Rise). PB and EMB denote Pigafetta and East Mariana basins, respectively.

frequent reversals occurring at rates similar to those of the Miocene [e.g., *Steiner et al.*, 1985; *Steiner and Ogg*, 1988; *Gradstein et al.*, 1994; *Ogg*, 1995; *Juárez et al.*, 1995; *Ogg and Gutowski*, 1996].

To gain a better understanding of the JQZ and to document its polarity reversal sequence, we undertook a study of the Pigafetta Basin anomalies using deep-tow magnetic profiles to increase the measured anomaly amplitudes and resultant signal-to-noise ratio. We chose Pigafetta Basin because there pre-M29 anomalies are best identified and mapped. With the magnetic sensor closer to the crustal source we were able to increase observed anomaly amplitudes by a factor of ~4. In this article we explore a polarity reversal model for these anomalies and its ramifications for the GPTS. Although we could not uniquely determine which anomalies result from reversals and which represent field fluctuations, our model implies both a rapid reversal rate and low magnetic field intensity during the Late Jurassic. It also provides a template for Jurassic magnetostratigraphic research. A more in-depth look at implications of the deep-tow data for the origin of the JQZ will be given in a later article (H. P. Johnson et al., in preparation, 1998).

2. Geologic Background

Our study area is a small part of the Pigafetta Basin located between seamounts of the Marcus-Wake group, centered at ~22°N, 152°E, where *Handschumacher et al.* [1988] first identified pre-M29 anomalies (Figure 1). This portion of Pacific plate formed at the NE-trending Pacific-Izanagi ridge during the Jurassic, as shown by M24 age and older magnetic lineations [*Handschumacher et al.*, 1988; *Nakanishi et al.*, 1989, 1992]. Additional evidence of Jurassic age is an Ar^{40}-Ar^{39} radiometric date of 166.8 ± 4.5 Ma from crustal basalts cored at Ocean Drilling Program (ODP) Site 801 (Figure 1) [*Pringle*, 1992]. Paleomagnetic data indicate that the region around ODP Sites 800 and 801(Figure 1) formed ~5°-12° south of the equator before drifting northward to its current location [*Steiner and Wallick*, 1992; *Wallick and Steiner*, 1992; *Larson et al.*, 1992; *Ito et al.*, 1995].

The most significant geologic event to occur in the Pigafetta Basin since its formation was a rash of mid-Cretaceous volcanism that affected much of the western Pacific [*Schlanger et al.*, 1981; *Larson*, 1991] forming several plateaus, numerous seamounts, and massive sills within the sediment column [*Larson and Schlanger*, 1981; Tarduno et al., 1991]. In our study area the few reliably dated seamounts have Ar^{40}-Ar^{39} radiometric dates that range from 95 to 119.6 Ma (Figure 1) [*Ozima et al.*, 1983; *Smith et al.*, 1989], consistent with Ar^{40}-Ar^{39} dates from other seamounts in the Marcus-Wake group [*Winterer et al.*, 1993]. Furthermore, drilling at ODP sites 800 and 802 cored basalt and dolerite sills whose Ar^{40}-Ar^{39} dates of 126.1 ± 0.6 and 114.6 ± 3.2 Ma, respectively [*Pringle*, 1992], imply that the sills were emplaced during this event. Although one might expect such volcanism to destroy the prior magnetic signature of the lithosphere, various studies have documented correlatable Jurassic and Early Cretaceous magnetic lineations in regions affected by the ubiquitous sills [e.g., *Larson and Schlanger*, 1981; *Nakanishi et al.*, 1992]. The survival of pre-Cretaceous anomalies is poorly understood, but two possible factors are (1) that the crust was not significantly remagnetized because source vents were limited in extent and the sills mainly intruded the sediment column and (2) the sills form a more or less uniformly magnetized, normal polarity sheet whose magnetic anomaly is small except over its edges [*Larson and Schlanger*, 1981].

Typical abyssal seafloor depths in Pigafetta Basin are ~5800 m with igneous basement lying beneath ~500-600 m of pelagic and volcaniclastic sediments [*Lancelot et al.*, 1990; *Abrams et al.*, 1993]. ODP Sites 800 and 801 were drilled in this area and multichannel seismic data collected in preparation for drilling have been used to define areas where the mid-Cretaceous sills are present (Figure 1). Most of these profiles over Pigafetta Basin show little seismic evidence of sill intrusions [Figure 1; *Abrams et al.*, 1993], suggesting this is a good location to examine the Jurassic magnetic lineations.

3. Data Collection

Magnetic data were collected along two subparallel tracklines using a three-axis deep-tow fluxgate magnetometer towed from the R/V *Thomas Washington* (cruise TUNE08WT). The two tracks are oriented nearly perpendicular to the magnetic lineations, and separated by 65-110 km (Figure 1). Track locations and directions were dictated by the lineation geometry and the need to avoid seamounts that surround the basin. The deep-tow sensor was towed at a depth of 4.5-5.0 km (Figure 2) at a speed of 2.1-2.5 kt (1.1-1.3 ms^{-1}), the depth and speed being a balance between the need to keep the sensor close to the source and the need to achieve maximum profile lengths. So that the magnetic profiles could be merged with accepted GPTS, the northwest ends of the two lines overlap M27 and M28, which are widely recognized chrons.

Surface magnetic data and single-channel seismic reflection data were collected over the southwestern two thirds of the deep-tow tracks during a weather hiatus (Figure 1), but inclement weather damaged the surface magnetometer sensor and seismic hydrophone array, making it impossible to collect surface magnetic and seismic reflection data simultaneously with the deep-tow data. SeaBeam multibeam echosounder data were collected along all lines yielding a swath of bathymetry ~4.5 km wide and allowing us to observe bathymetry slightly to the sides of the ship tracks.

4. Magnetic Data Processing

Raw total field magnetic measurements were processed through the following steps: (1) filtering, (2) gridding, (3) diurnal variation removal, (4) continuation to a level datum, (5) regional field correction, (6) projection to a common azimuth, and (7) deskewing (reduction to the pole). In the first step a median filter [*Press et al.*, 1986] was applied to remove noise caused by a faulty bit in the magnetometer's analog-digital converter. This problem generated spurious readings whose values usually differed greatly from valid measurements. Because the magnetic profiles are highly over sampled, it was possible to remove bad readings by calculating a moving-window median value and rejecting values outside a specified range. Even with these deletions, the resulting data set was large, so a cubic spline was fit to the data to reduce the readings to a manageable number and to resample them on a regular grid.

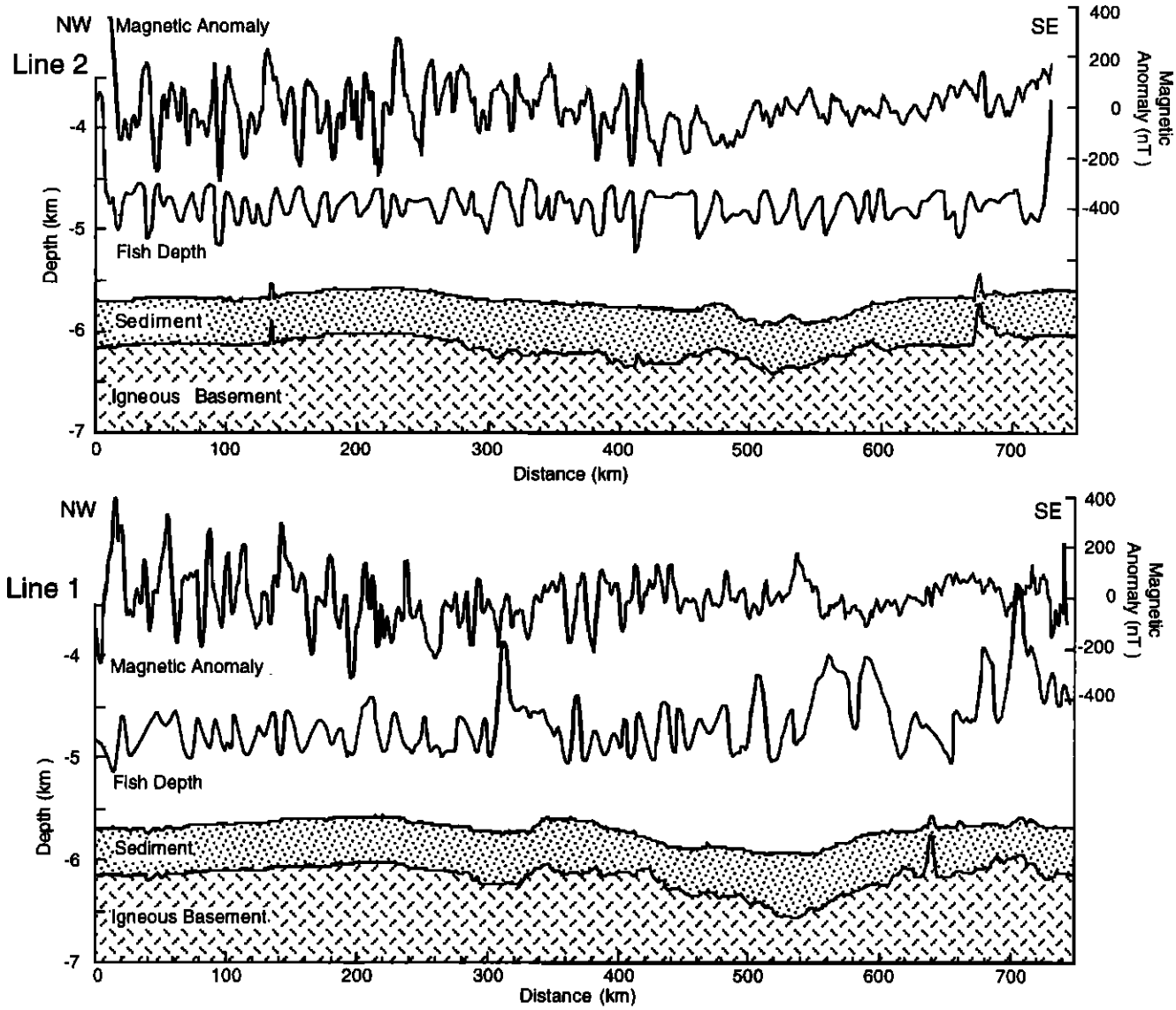

Figure 2. Magnetic anomalies and profiles of magnetometer sensor, seafloor, and basement depth along the two deep-tow tracks. Line 1 is the southernmost of the two. Sediment thicknesses were determined from single-channel seismic data collected on cruise TUNE08WT, where available, and figures from prior multichannel seismic data tracks [*Abrams et al.*, 1993], where available. A constant sediment thickness was assumed where seismic data were unavailable. The deep-tow magnetic data in this figure have not been deskewed (see text), although effects of fish depth and diurnal magnetic field variations have been removed. Note that the apparently sharp depth variations of the magnetometer sensor are mainly a result of the high vertical exaggeration (70:1).

Low-frequency external field variations, mainly the solar diurnal effect, were estimated using records from magnetic observatories at Guam and Honolulu. Because the Guam station is closest to the study area (13.4°N, 144.7°E, 1150 km away), that record was low-pass filtered, shifted in time by the difference in solar time between the station and ship locations, and scaled by a linear interpolation between the Guam and Honolulu diurnal range values. This assumes that long-period field variations are similar over distances of ~1000 km and that the decrease in daily range with magnetic latitude is approximately linear between the two stations [e.g., *Onwumechilli*, 1967]. Calculated daily ranges range from 30 to 73 nT but average 54 nT.

Although we attempted to keep the magnetometer sensor at a constant depth, this varied owing to surface weather, ship's speed, and currents. With few exceptions we were able to maintain the sensor within a depth range of ~500 m while limiting the frequency of depth oscillations to ~10-20 km (Figure 2). Although the effect of most sensor depth variations on the magnetic data was small, only a few tens of nanoTeslas, we corrected these by variable continuation of the magnetic values from an irregular surface to a level datum of 4.5 km [*Guspi*, 1987]. Regional field variations were removed by reducing the data to the 1985 International Geomagnetic Reference Field. Differences in ship track direction were addressed by projecting the data to a common azimuth of 305°, perpendicular to the magnetic lineations.

Magnetic lineation shapes are typically asymmetric relative to the source body because this depends, among other things, on the relationship of ambient magnetic field

direction, remanent magnetization, and lineation azimuth [*Schouten*, 1971]. In the case of the Pigafetta lineations, reversely polarized crust produces a positive anomaly because it formed in the southern hemisphere and drifted across the equator [*Larson and Chase*, 1972]. We corrected this bias by deskewing the deep-tow profiles using a reduction-to-the-pole method based on Fourier domain filtering [*Schouten and McCamy*, 1972], which makes the anomalies symmetric over their source blocks and places positive anomalies over normally magnetized blocks. To apply this technique, one must assume the remanent magnetization direction or determine it empirically by trial and error. We tried both approaches, but the empirical method was not reliable owing to interference among closely-spaced anomalies (the "sequence effect" of *Dyment et al.* [1994]). Instead, we calculated a skewness parameter, Q = -176°, using the ambient field inclination and declination of 27° and 3°, respectively, and assuming a paleolatitude of 5°S and a paleodeclination of 20°. These values are consistent with Pacific paleomagnetic data of Jurassic age [*Hildebrand and Parker*, 1987; *Sager*, 1992; *Larson and Sager*, 1992; *Larson et al.*, 1992]. Although the Pacific Jurassic paleolatitude and paleodeclination values are uncertain by 10°-15° [*Sager*, 1992; *Larson et al.*, 1992], the deskewed profiles are not sensitive to differences of this magnitude.

5. Constructing a Polarity Series

5.1. Magnetic Model

Our approach to making a polarity time series for the Jurassic deep-tow profiles was to use a simple two-dimensional magnetic model of the crust [*Talwani and Heirtzler*, 1964], assuming a constant 1 km thickness of the magnetic layer and vertical polarity boundaries. We moved polarity block boundaries and adjusted magnetization strength to produce a satisfactory match of observed and calculated magnetic anomalies. Although *Cande and Kent* [1992a] showed that magnetic modeling is not necessary because zero crossings of deskewed anomalies can be used to define polarity boundaries, our data contain many small anomalies and some long-wavelength variations that make it difficult to define anomaly boundaries simply by zero crossings.

Oceanic crustal magnetization structure is probably complex, having contributions from deeper layers and finite, nonvertical polarity boundaries (see reviews by *Smith* [1990] and *Dyment and Arkani-Hamed* [1995]). Therefore we also tried models with different parameters or greater complexities to see whether changing the source layer thickness, adding additional layers, or using Gaussian polarity transitions of varying thickness (i.e., finite-width transitions) would significantly improve the match of calculated and observed anomalies. Although most models can be improved by adding additional parameters, the small improvements were considered not worth the additional model complexities. In addition, calculations of ocean crust magnetization derived from combined mineralogy and thermal models justify our method by indicating that at fast spreading rates the crustal magnetization is remarkably similar to a simple rectangular block model [*Dyment and Arkani-Hamed*, 1995].

Depth to igneous basement (Figure 2) was determined using the single-channel seismic reflection profiles collected over the southwestern two thirds of the deep-tow lines. Because these data and multichannel profiles [*Abrams et al.*, 1993] in the area indicate an approximately uniform layer of sediments, we assumed a constant-thickness sediment cover of the same depth on the northwestern third of the lines where seismic reflection data were unavailable (Figure 2).

In the deep-tow version of the model we used a magnetization intensity that decreased exponentially with horizontal distance ($M = M_0 \cdot e^{-[x \cdot 0.0025]}$, with $M_0 = 2.25$ Am^{-1}) towards older seafloor to approximate the decrease of anomaly amplitude in the same direction (Figure 3). This function was determined qualitatively, thus no special importance should be attributed to the specifics of this approximation other than its indication of decreasing anomaly amplitude. In the model of anomalies upward continued to the sea surface we reproduced the longer-wavelength anomalies on the southeast ends of the profiles. Because these do not show as great a decrease in amplitude as do the short-wavelength anomalies, the magnetization function was divided into two parts. For the northwest ends of the profiles the same exponential was used where it gives anomaly magnetizations >1 Am^{-1}. A constant value of 1 Am^{-1} was used for older anomalies located to the southeast.

Magnetic anomalies were modeled at two depths, 4.5 km below sea level and upward continued to the sea surface. The latter was used to create a polarity model directly comparable with previous GPTS derived from data acquired at or near the sea surface. Polarity boundaries were modeled with a resolution of 250 m, a value chosen to be small enough to easily represent all of the features of the anomalies. Although this made it possible to represent even very small amplitude features, anomalies whose amplitudes were <10% of the peak-to-peak amplitudes of the dominant anomalies nearby were not modeled because we felt they were likely to be caused by paleointensity fluctuations rather than reversals. Although this criterion was somewhat arbitrary, it is common practice to ignore some or all of the smallest anomalies. The polarity model contains blocks ranging in width from 250 m to ~16 km (Figure 4).

5.2. Correlation and Composite Model

We next combined the two models of polarity versus distance, one for each of the two deep-tow lines, into a composite series (Figure 4). The purpose was to retain only those blocks that create anomalies that can be correlated between lines and to use the redundancy of two sequences to reduce errors in the polarity record caused by local geology and structural variations. To make this twofold stack, it was necessary to make a detailed correlation of individual anomalies between lines (Figure 5). In matching anomalies we examined several different depth representations of the data. The composite aeromagnetic profile of *Handschumacher et al.* [1988] was compared with our deep-tow profiles at 4.5 km depth as well as profiles upward continued to 2.5 km depth and the sea surface (Figure 5). Upward continuation acts as a low-pass filter, so examining changes in the character of the anomalies at different depths made it possible to infer which sets of deep anomalies combine to form sea surface anomalies.

In general, the correlation of anomalies between profiles was good, with 69% and 80% of the modeled blocks from lines 2 and 1, respectively, matching in the composite. Polarity blocks that were not correlated from one line to the other were deleted from the composite series (Figure 4). Some parts of

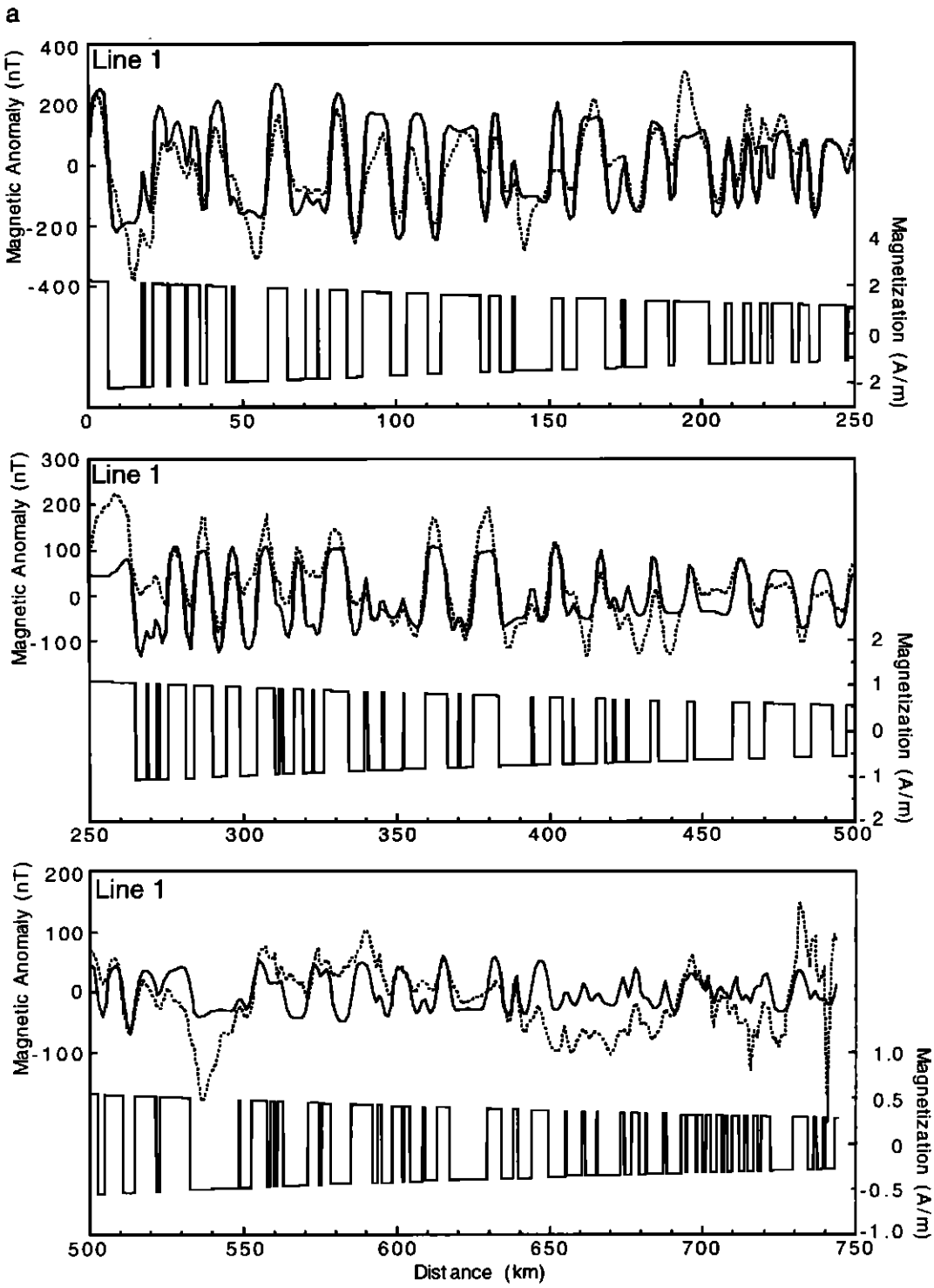

Figure 3. Magnetic polarity block model of the deep-tow magnetic profiles. Figures 3a and 3b are each broken into three panels for clarity. The dashed and solid lines represent the observed and calculated magnetic anomalies, respectively, whereas the damped square wave at the bottom of each panel gives the magnetization. Observed magnetic profiles have been deskewed.

the profiles were more easily matched than others. Anomalies in the 0-400 km range (M27-M35) correlated most easily because the peaks have the most similar characteristics (Figures 4 and 5). At ~450-500 km, anomalies M36 and especially M37 showed differences in shape and spacing that made correlation difficult. Older, smaller amplitude anomalies show a striking regularity of period and amplitude that make it difficult to correlate by distinctive characteristics (Figures 4 and 5). Nevertheless, the positions of these anomalies relative to the longer-wavelength features, especially in the

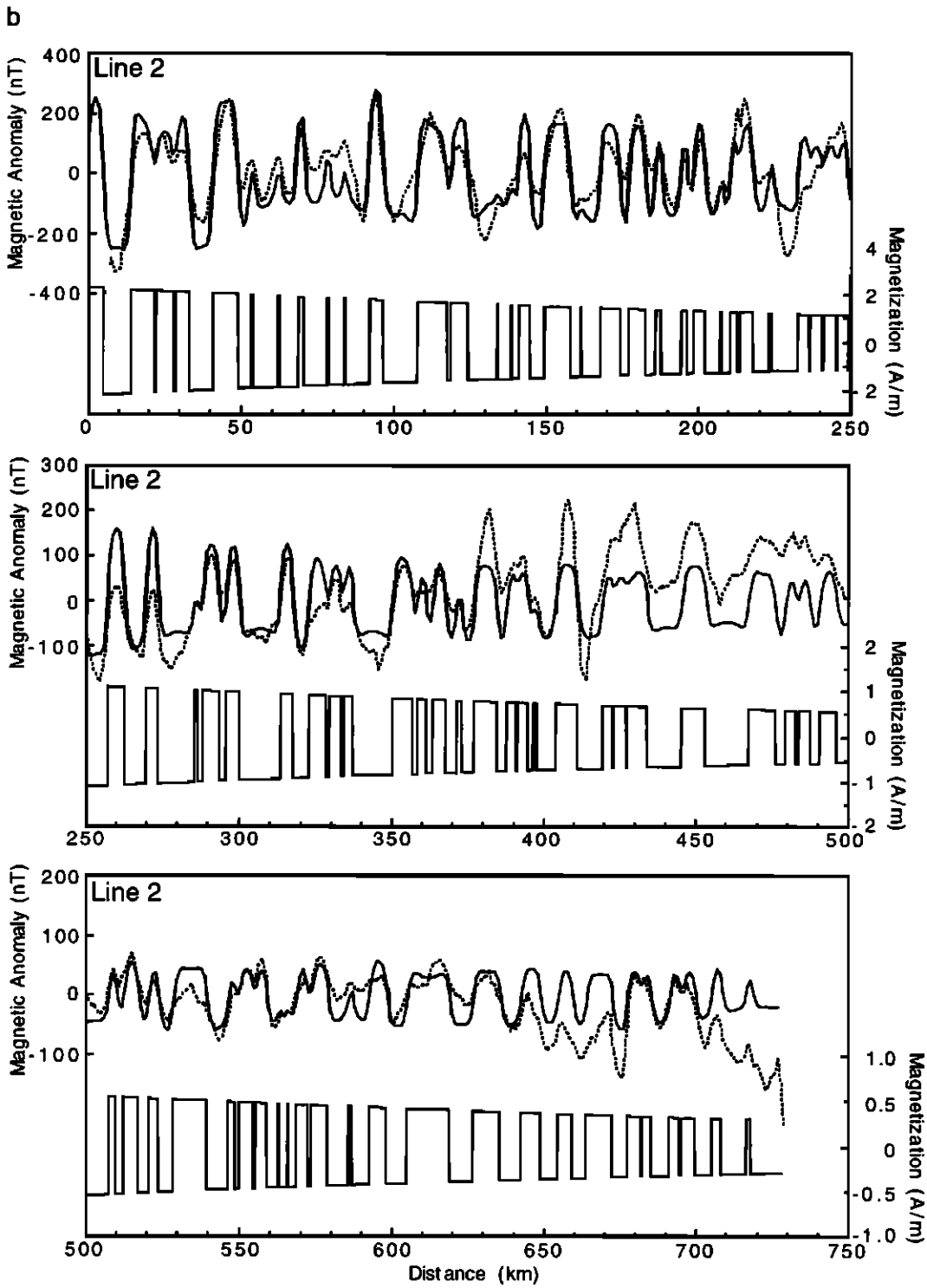

Figure 3. (continued)

2.5 km upward continued profiles, made it possible to make nearly a one-to-one correlation of these anomalies. Although we are confident of our matching of these anomalies, the regularity of their spacing makes it possible that our correlation could be off by one anomaly peak but doubtfully more.

After correlation and stacking, two additional adjustments were made to the final polarity block model. Since some short-wavelength blocks survived the correlation process, we considered whether the shortest-wavelength anomalies are caused by crustal magnetization or chance correlation of artifacts. Lognormal plots of spectral amplitudes calculated from the deep-tow profiles (Figure 6) showed two approximately linear sections with a break in slope at ~0.7 km^{-1} (1.4 km wavelength). This shape is typical of spectra of an ensemble of uncorrelated magnetic bodies with the slope of the longer-wavelength section being related to the depth of the magnetic source [*Spector and Grant*, 1970; *Kovacs and*

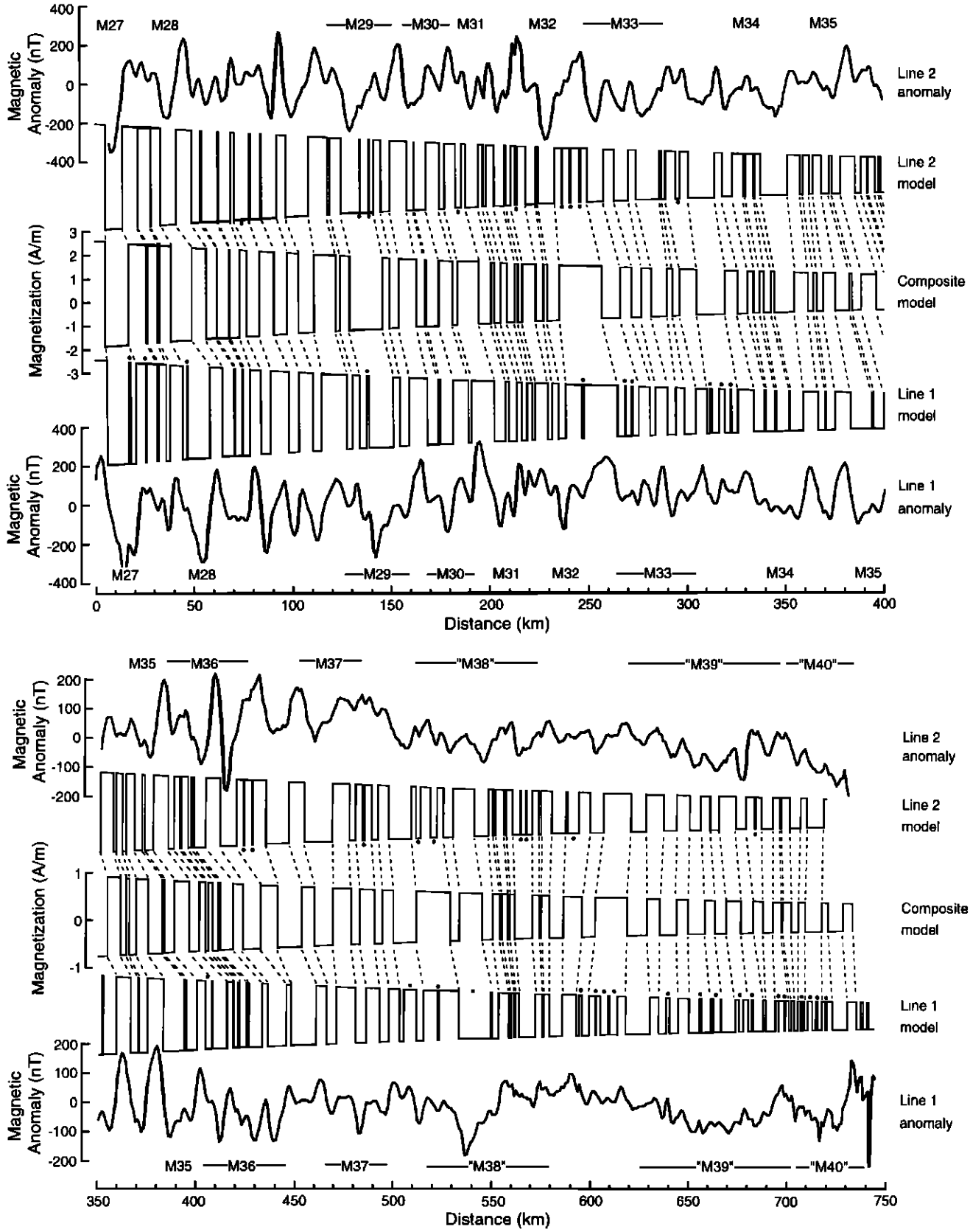

Figure 4. Composite polarity series made from stacking the models of the two deep-tow profiles. At the middle is a square wave representation of composite magnetization, flanked at the top and bottom by the magnetization functions for the two lines. The upper and lower solid curves are deskewed deep-tow magnetic profiles, for comparison. Dashed lines show correlations between polarity series. Dots beneath (above) the magnetization functions of line 2 (line 1) show anomalies that could not be correlated. Crosses on the composite magnetization curve show short polarity periods that were dropped from the final model (see discussion).

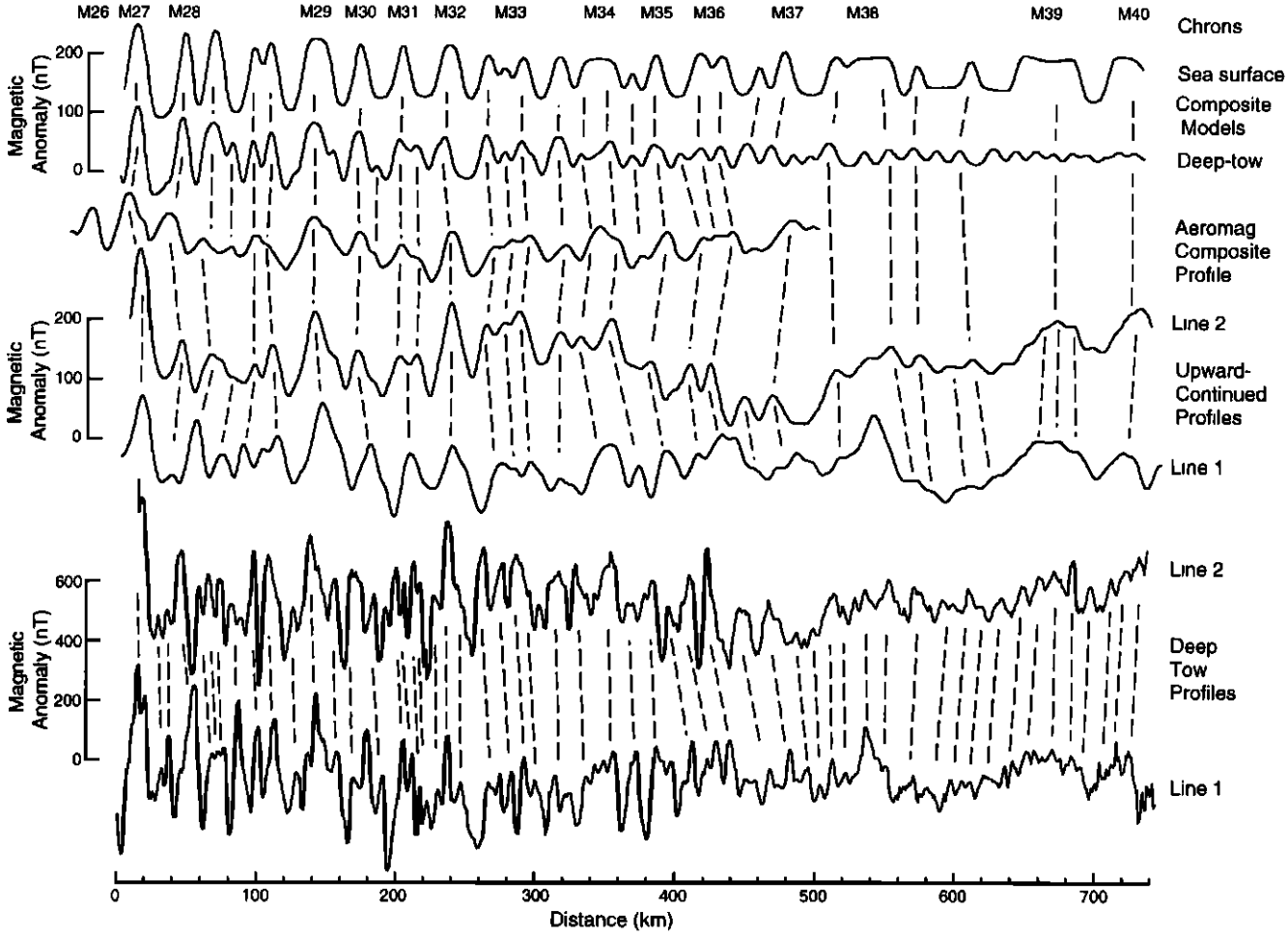

Figure 5. Correlation of magnetic profiles. The bottom four curves show the deep-tow profiles at 4.5 km depth and upward continued to the sea surface. At the top are the composite aeromagnetic profile redrawn from that published by *Handschumacher et al.* [1988] and calculated profiles from the deep-tow and sea surface models. Dashed lines between profiles denote correlations. The difference between the two versions of the magnetic model is that one was calculated to match the deep-tow profiles whereas the other was adjusted to fit the upward continued deep-tow profiles For comparison with prior data these magnetic anomalies have not been deskewed.

Vogt, 1982]. The almost flat short-wavelength section is usually interpreted as the signature of data containing a significant noise component [e.g., *Parker*, 1997]. Thus we considered it inappropriate to retain polarity blocks <1.4 km in length, corresponding to a period of 22 kyr (see section 6).

The second adjustment was in response to the poor comparison of calculated anomalies upward continued to the sea surface with the composite aeromagnetic profile of *Handschumacher et al.* [1988] (Figure 5). In the deep-tow anomaly model, short-wavelength anomalies on the southeast ends of the lines are considered to be caused by polarity blocks (Figure 4). Because the source and observation datum are close, the deep-tow model could not easily reproduce the longer wavelength anomalies evident in the sea surface versions (Figure 5). Consequently, we made a "sea surface" model by taking the two line models (Figure 3) and modifying the polarity blocks to make a better match of the upward continued profiles at the sea surface. The modifications mostly consisted of deleting polarity blocks whose anomalies are not represented in the upward continued data, but a few block boundaries were also moved short distances laterally. As a result, the sea surface model is not simply a low-pass filtered version of the deep-tow model. Furthermore, this modeling is not exactly equivalent to modeling sea surface profiles because the signal-to-noise ratio has been enhanced by acquiring data closer to the magnetic source.

6. Age Calibration

Few good absolute age calibration points exist for the M-series magnetic anomalies. Most GPTS use either two points, one around M0 and the other around M25 [e.g., *Kent and Gradstein*, 1985; *Harland et al.*, 1990; *Gradstein et al.*, 1994], or three points with another near M11 [*Channell et al.*, 1995]. All chrons between these points have ages which are linearly interpolated. Because our anomalies are older than the oldest calibration point, we follow previous investigators [e.g., *Cande et al.*, 1978; *Handschumacher et al.*, 1988] and calculate the ages of Jurassic chron boundaries by linear extrapolation from the accepted anomalies.

To use this approach, we need a spreading rate and a tie point. Both were determined from a sea surface magnetic

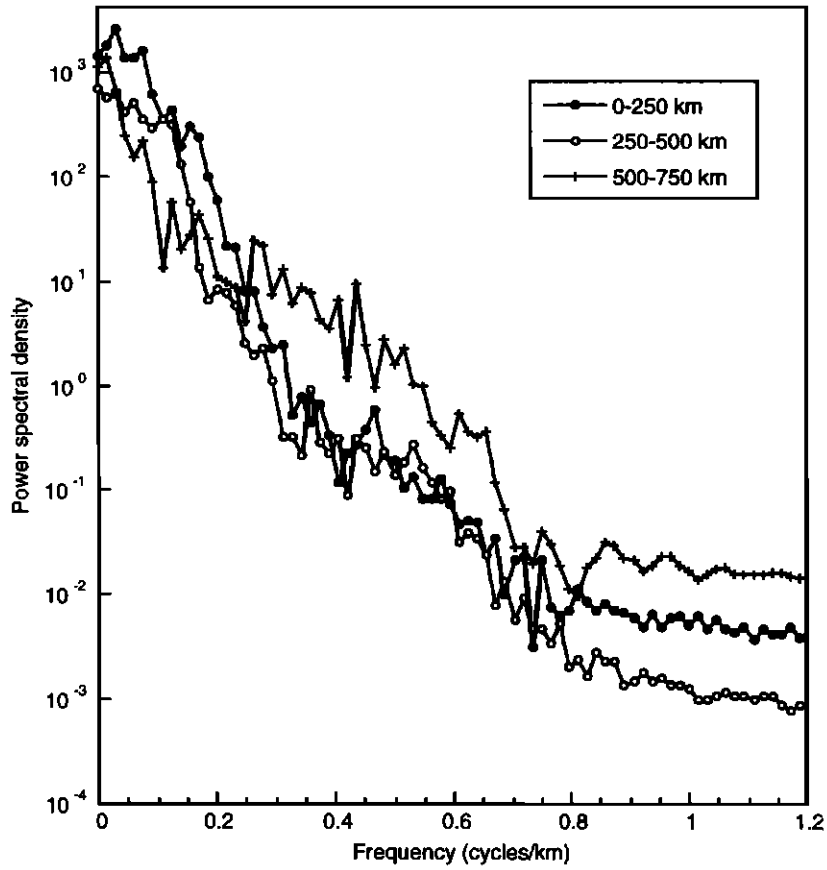

Figure 6. Power spectra of three segments of Line 1. Horizontal scale is linear whereas vertical scale is logarithmic. We interpret the break in slope at 0.7 km^{-1} as the transition from signal to nearly random noise.

profile from a prior cruise (D/V *Glomar Challanger*, Leg 89; see Figure 1) which crosses the younger of the deep-tow anomalies in addition to younger anomalies (M24-M29) in accepted GPTS. We projected this profile normal to the lineations, deskewed it, and made a polarity model (Figure 7). To determine the half spreading rate, polarity block boundary ages from various GPTS were plotted versus distance and a least squares line was calculated to determine the slope (Figure 8). The correlation coefficient for the preferred line is 0.99, implying a constant spreading rate over this time interval.

M-series calibration ages have changed significantly in recent GPTS, so the calculated half spreading rates vary by 50%, from 44.0 to 65.0 mma^{-1} (Figure 8). We prefer the latter rate, inferred from the *Harland et al.* [1990] GPTS, because this GPTS used a recent, more acceptable age for M0 and it predicts ages that agree well with radiometric dates of 155.3 ± 3.4 Ma for M26r (ODP Site 765 in the Argo Abyssal Plain) [*Ludden*, 1992] and 166.8 ± 4.5 Ma for ODP Site 801 [*Pringle*, 1992] in Pigafetta Basin (Figure 8). We could have used these two radiometric ages as tie points [e.g., *Ogg*, 1995] and interpolated anomaly ages in between, but we felt this would place undue significance on these two ages. Both ages have large standard errors, and the younger is from hydrothermal minerals that may have been precipitated sometime after the crust and its magnetic signature were formed [*Ludden*, 1992]. This procedure will produce a change in slope of the anomaly versus age curve where the Jurassic timescale is attached to the younger GPTS and this would give rise to artifacts in interpretations made from using this composite GPTS.

Our tie point to the younger GPTS was the old boundary of Chron M27r (see the appendix). Making another choice for the base GPTS would change the calculated polarity boundary ages with consequent changes in the details of our interpretations; nevertheless, the changes would be incremental and would not lead to significantly different conclusions. To allow readers to adapt our polarity model to improved GPTS, we provide the polarity boundary distances used in this calculation (see the appendix). Magnetic boundary ages for the deep-tow model are given in Table 1, whereas Table 2 contains boundary ages for the model of anomalies upward continued to the sea surface.

Our GPTS are compared in Figure 9 with that given by *Handschumacher et al.* [1988]. Our deep-tow-derived timescale (Figure 9) shows eleven short polarity periods that are not included in the *Handschumacher et al.* [1988] timescale. These come from short-wavelength anomalies that merge with others and disappear when continued to the sea surface. These short period polarity blocks occur more-or-less evenly throughout the timescale (in M28, M29, M30, M31, M32 (2), M34 (3), and M37). The deep-tow timescale shows numerous short polarity periods before M37 which resulted from our modeling the many small anomalies on the southeast ends of the profiles. If valid, these imply an extremely high reversal rate of the order of 12 reversals per million years, whereas the sea surface model implies a reversal rate which is reduced by half and similar to that from other GPTS (Figure 10). The sea surface model timescale contains fewer polarity chrons (Figure 9) because short chrons were lost in upward continuation.

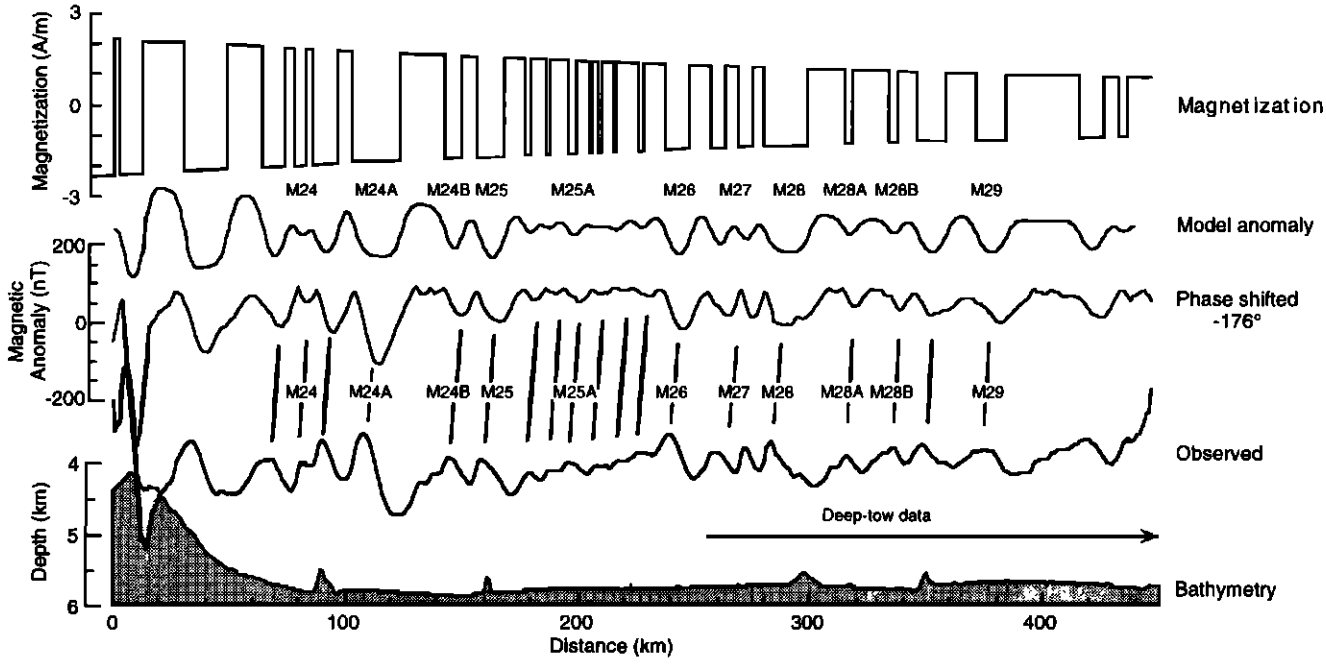

Figure 7. Magnetic model of D/V *Glomar Challenger* Leg 89 magnetic profile which was used to connect the magnetic model of pre-M26 magnetic anomalies with the magnetic polarity timescale of younger anomalies. From bottom to top, curves are bathymetry, observed magnetic anomaly, deskewed magnetic anomaly, calculated model anomaly, and magnetization model. Vertical lines show the correlation of skewed and phase-shifted anomalies, and numbers give identification. The arrow shows the region of overlap with deep-tow data. Track location is shown in Figure 1.

This version of the polarity sequence is similar to that of *Handschumacher et al.* [1988]. Our GPTS misses a few short polarity periods recognized by *Handschumacher et al.* [1988] because these anomalies did not correlate between our profiles and consequently were not represented in the model. The main differences between our and the Handschumacher et al. GPTS are that the same chrons span a shorter time in our timescale, a result of the faster spreading rate inferred from newer M-series calibrations, and the addition of new anomalies M38-M41.

7. Discussion

The deep-tow data presented here not only provide a basis for extending the marine magnetic anomaly-based GPTS but also give new insights about field behavior during the Jurassic Quiet Zone. They allow us to extend the GPTS into the Jurassic about 9 m.y. past M29, and they imply abundant magnetic reversals occurring at a rapid rate. Two models were considered owing to the difficulty in determining which anomalies result from polarity reversals. In one model we presumed all of the correlatable anomalies were caused by reversals. In the other we assumed that only the largest represent reversals and the remainder are paleointensity fluctuations.

Although it is usual to represent all correlatable anomalies by reversals when constructing a GPTS, we should examine this assumption closely. At first it seems an appropriate approximation because most polarity chrons attributed to large magnetic anomalies have been verified by magnetic stratigraphy. Small anomalies, termed "tiny wiggles" [*LaBrecque et al.*, 1977], are a different matter. Tiny wiggles have been noted in many parts of the marine anomaly sequence [*Blakely and Cox*, 1972; *Blakely*, 1974; *Rea and Blakely*, 1975; *Cande and LaBrecque*, 1974; *Wilson and Hey*, 1981; *Cande and Kent*, 1992b]. A few can be verified as resulting from polarity reversals [*Rea and Blakely*, 1975; *Wilson and Hey*, 1981; *Clement and Kent*, 1987], but most have not. *Cande and Kent* [1992b] suggest that the signature of many of these anomalies is more consistent with paleointensity fluctuations than polarity reversals and argue that they are probably ubiquitous in magnetic profiles. Although they state that tiny wiggles may also be useful for time calibration, we do not wish to misinterpret tiny wiggles as reversals in a GPTS.

Cande and Kent [1992a] removed all chrons shorter than 30 kyr duration from their GPTS arguing that these short features probably represent paleointensity fluctuations. However, the separation of true polarity chrons from intensity fluctuations based on length is probably impossible. Even though paleointensity fluctuations may have shorter characteristic periods than true reversals, their period distributions clearly overlap. Paleointensity records covering the last 140-200 kyr yield dominant frequencies of ~24 kyr [*Meynadier et al.*, 1994], but marine records imply paleointensity variation periods >100 k.y. [Cande and LaBrecque, 1974]. In comparison, short-period polarity reversals, such as the Réunion and Cobb Mountain subchrons, have been documented with durations of 10-30 kyr [*Gromme and Hay*, 1971; *Rea and Blakely*, 1975; *Clement and Kent*, 1987]. Moreover, statistical analysis of GPTS indicates that reversals and paleointensity fluctuations likely result from the same set of geomagnetic instabilities [*Marzocchi*, 1997], implying that they likely appear similar in magnetic profile data.

Our profiles give few clues as to which anomalies are a result of reversals and which are a result of paleointensity fluctuations. Examining the young ends of our profiles

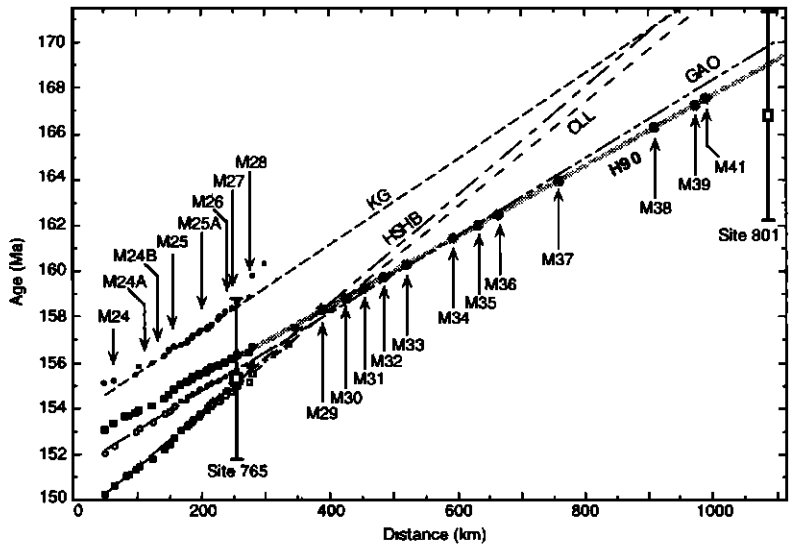

Figure 8. Determination of the spreading rate and ages for the deep-tow magnetic profile models. Symbols at left denote chron boundaries (M24-M28) on the D/V *Glomar Challenger* Leg 89 profile that overlaps deep-tow profiles (Figure 1). For comparison, dates and 1 standard deviation error bars are shown for Chron M26r at ODP Site 765 in the Argo Abyssal Plain (155.3 ± 3.4 Ma [*Ludden*, 1992]) and Site 801 (166.8 ± 4.5 Ma [*Pringle*, 1992]), located southeast of the deep-tow lines. Least squares lines were fit to chron boundaries using ages from various geomagnetic polarity reversal timescales (GPTS) to derive spreading rates which were extrapolated over older seafloor to give chron boundary ages for the deep-tow models. The preferred age model given by the *Harland et al.* [1990] GPTS (heavy line) is most consistent with seafloor ages from Sites 765 and 801. Shaded circles show extrapolated ages for main modeled chrons. Dashed lines show extrapolated ages for other GPTS (CLL, Cande et al. [1978]; KG, Kent and Gradstein [1985]; HSHB, Handschumacher et al. [1988]; H90, Harland et al. [1990]; GAO, Gradstein et al. [1994]).

(Figure 5), one could easily conclude that the anomalies result from polarity reversals, since M27-M30 have been verified by magnetic stratigraphy [*Steiner et al.*, 1985; *Juárez et al.*, 1995]. Additionally, magnetostratigraphic results from Europe, while not continuous enough to verify any of these chrons in particular, demonstrate that the geomagnetic field was reversing during most of the period covered by our model [*Steiner and Ogg*, 1988; *Ogg*, 1995; *Ogg and Gutowski*, 1996]. On the other hand, one might conclude that the small amplitudes and short wavelengths on the old ends of our profiles indicate that those anomalies are caused by paleointensity fluctuations. Magnetostratigraphic data for the part of the Jurassic corresponding to ~M38 and older are lacking [*Ogg*, 1995], so we cannot document whether reversals actually occurred during this time. The characteristic wavelengths of the short-wavelength anomalies on the old ends of our profiles, ~10-20 km, correspond to periods of 150-300 kyr, similar to those suggested for paleointensity variations by other marine anomaly records [*Cande and LaBrecque*, 1974].

Although magnetic results from nearby ODP Hole 801C (Figure 1) are somewhat contradictory, they provide possible clues to the significance of the oldest of our tiny wiggles. Approximately 100 m of alkali and tholeiitic basalts, thought to be from the uppermost oceanic crust, were cored at this site [*Floyd and Castillo*, 1992]. Paleomagnetic inclination data indicate five polarity blocks within the section and imply that the JQZ may be caused by partial cancellation of the magnetic anomalies owing to the superposition of different polarity layers [*Wallick and Steiner*, 1992]. In contrast, downhole magnetometer results indicate that only two of the polarity blocks are primary and that the others are likely a secondary magnetization acquired because of hydrothermal alteration [*Ito et al.*, 1995]. Because the alkalic basalt section was probably emplaced after crustal formation and may have caused hydrothermal metamorphism of the older crust [*Floyd and Castillo*, 1992; *Alt et al.*, 1992], this hypothesis is plausible. Thus the small anomalies on our profiles in the vicinity of Site 801 probably reflect paleofield behavior, rather than complex crustal magnetic structure.

Perhaps more significant are measurements of natural remanent magnetizations from Site 801 basalts. The 36 m alkali and 63 m tholeiitic sections have log average magnetizations of 1.24 Am^{-1} and 2.30 Am^{-1}, respectively [*Wallick and Steiner*, 1992]. These values are significantly greater than the 0.35 Am^{-1} calculated magnetization at the old end of our deep-tow model. The magnetization strength of our model is poorly constrained owing to the nonuniqueness of the model. For example, halving the source layer thickness would double the intensity but increasing it by a factor of 7 by decreasing the thickness would require an unreasonably thin source layer.

Relative to the thickness of the crustal magnetic source, the Site 801 section is short, so it is possible that the sample magnetizations overestimate the average magnetization. Such cores typically do not recover the interflow breccias, hyaloclastites, clays, and other less magnetic material that would reduce the overall magnetization. Furthermore, if polarity reversals occur within the crust, this also will lessen the effective magnetization [*Johnson and Merrill*, 1978]. Nevertheless, the difference between our deep-tow model and the observed magnetization is so large that it requires an

Table 1. Deep-tow Reversal Model Boundaries and Ages

Distance, km		Age, Ma		
Young	Old	Young	Old	Chron
5 500	17.250	156.229	156.410	M27r
38 750	49 500	156 741	156 906	M28r
56 625	73.375	157.016	157.273	M28Ar
77.000	83.250	157 329	157.425	M28Br
90.875	97 375	157.543	157.643	M28Cr
103.125	111 000	157 731	157 852	M28Dr
122.125	124 250	158.023	158 056	M29n.1r
129 000	145 875	158.129	158 389	M29r
149.375	154 125	158.443	158 516	M29Ar
163 000	174 500	158.652	158 829	M30r
181 625	183 875	158 939	158 973	M30Ar
195.000	200 875	159 145	159 235	M31n.1r
202.875	205 875	159.266	159 312	M31n2.r
209.000	212 875	159.360	159.420	M31r
214.500	216 625	159.445	159 477	M32n.1r
223 625	227 375	159.585	159.643	M32n.2r
229.500	235.500	159.675	159 768	M32r
256.750	266 250	160.095	160 241	M33r
271 875	276 875	160.327	160 404	M33Ar
281 750	289 875	160.479	160 604	M33Br
292 625	296 375	160.647	160 704	M33Cn.1r
305.125	319 750	160.839	161.064	M33Cr
325 875	331 000	161 158	161.237	M34n.1r
334.375	337 125	161 289	161 331	M34n.2r
339 375	343.000	161 366	161 422	M34n.3r
344.625	354 625	161.447	161.600	M34Ar
361 500	364 125	161 706	161 747	M34Bn 1r
365.875	369 000	161.773	161 822	M34Br
375 250	388.500	161 918	162.122	M35r
396 250	401.375	162 241	162.320	M36n 1r
404 500	406.000	162.368	162.391	M36Ar
408.125	418 250	162.423	162.579	M36Br
423 250	432.125	162.656	162 793	M36Cr
449.500	457 750	163 060	163 187	M37n.1r
466 500	476.250	163 322	163 472	M37r
484 125	488.125	163.593	163.654	M38n 1r
495.000	497 625	163.760	163.800	M38n.2r
503.375	511 000	163.889	164.006	M38n.3r
528 125	532.875	164 270	164.343	M38n.4r
543.375	549.625	164.504	164 600	M38r
561.000	570.000	164.775	164.914	M39n.1r
578.625	585 375	165.047	165.150	M39n.2r
594 875	601.500	165.297	165.398	M39n.3r
617.750	627.875	165.648	165.804	M39n.4r
634.625	643.000	165 908	166.037	M39n.5r
649.000	657.500	166.129	166 260	M39n 6r
662.500	668 375	166.337	166.427	M39n 7r
675 750	682.125	166.541	166 639	M39r
686.750	692.000	166.710	166 791	M40n.1r
701.125	704.750	166.931	166.987	M40n 2r
708.125	716.500	167.039	167.168	M40n 3r
720 000	727 250	167.222	167.333	M40r
732 000		167.406		M41r

Reversed polarity periods

implausible combination of factors to decrease the bulk crustal magnetization and increase the model magnetization. In contrast, our sea surface model has a magnetization intensity of 1 Am^{-1} at the old ends of the profiles, and this could easily be increased to 2 Am^{-1} by making the reasonable assumption that the main source layer is half as thick (500 m). Indeed, many magnetic profiles have been modeled with a source layer having approximately this thickness [e.g., *Blakely and Cox*, 1972]. If we accept this hypothesis, it implies that many of the small magnetic anomalies on the southeast ends of our profiles were not caused by magnetic reversals.

Given these considerations, we present our models with a caveat: the sea surface model likely underestimates the number of polarity chrons by leaving out the shorter ones, and the deep-tow model probably includes some paleointensity variations misinterpreted as polarity chrons. This problem is shared with all GPTS: for example, *Marzocchi* [1997] estimates that 35%-65% of short duration polarity chrons are missing from existing sea surface data derived GPTS. As a template for future magnetostratigraphic research, our sea surface model may be the more viable because it is a more conservative interpretation and is consistent with other sea surface models.

Our study of Pigafetta Basin deep-tow magnetic anomalies has provided insights to the nature of JQZ geomagnetic field behavior. The JQZ appears to be neither a result of constant polarity nor polarity chrons so closely spaced as to cancel from upward continuation to the sea surface. Our model requires a substantial increase in magnetization intensity with time beginning at least at anomalies M34-M35 and extending 20 m.y. to M21 time. We favor a geomagnetic cause for this behavior for several reasons. If it were a result of crustal formation or deterioration processes, then this process must

Table 2. Sea Surface Reversal Model Boundaries and Ages

Distance, km		Age, Ma		
Young	Old	Young	Old	Chron
3.563	18.250	156.199	156 425	M27r
40.375	49 875	156.766	156.912	M28n.1r
59.625	72.875	157.062	157.266	M28n.2r
90.125	97.750	157.531	157.648	M28n.3r
101.125	110.875	157.700	157 850	M28r
128.125	149.875	158.116	158.450	M29r
164.750	174.500	158.679	158.829	M30r
196.125	204.875	159.162	159.297	M31r
226 125	242.625	159.623	159.877	M32r
256.750	266.875	160.095	160.250	M33n 1r
270 625	276 750	160.308	160.402	M33n.2r
281.250	291.875	160.472	160 635	M33n 3r
306 375	319 750	160.858	161.064	M33r
325.875	355.250	161.158	161.610	M34n 1r
361 375	367 000	161.704	161.791	M34r
375.250	386.125	161.918	162.085	M35r
405 500	419 750	162.383	162.602	M36n.1r
422.500	433.625	162.645	162 816	M36r
452.750	457.375	163.110	163.181	M37n 1r
467.625	478.250	163.339	163.502	M37r
503.625	515.250	163.893	164.072	M38n.1r
517.000	551 625	164.098	164.631	M38r
564.250	569.250	164 825	164.902	M39n.1r
603.000	607.875	165.422	165 497	M39n 2r
638.000	684.125	165.960	166.670	M39r
703.125	728.125	166 962	167 347	M40r
739.125		167.516		M41r

Reversed polarity periods.

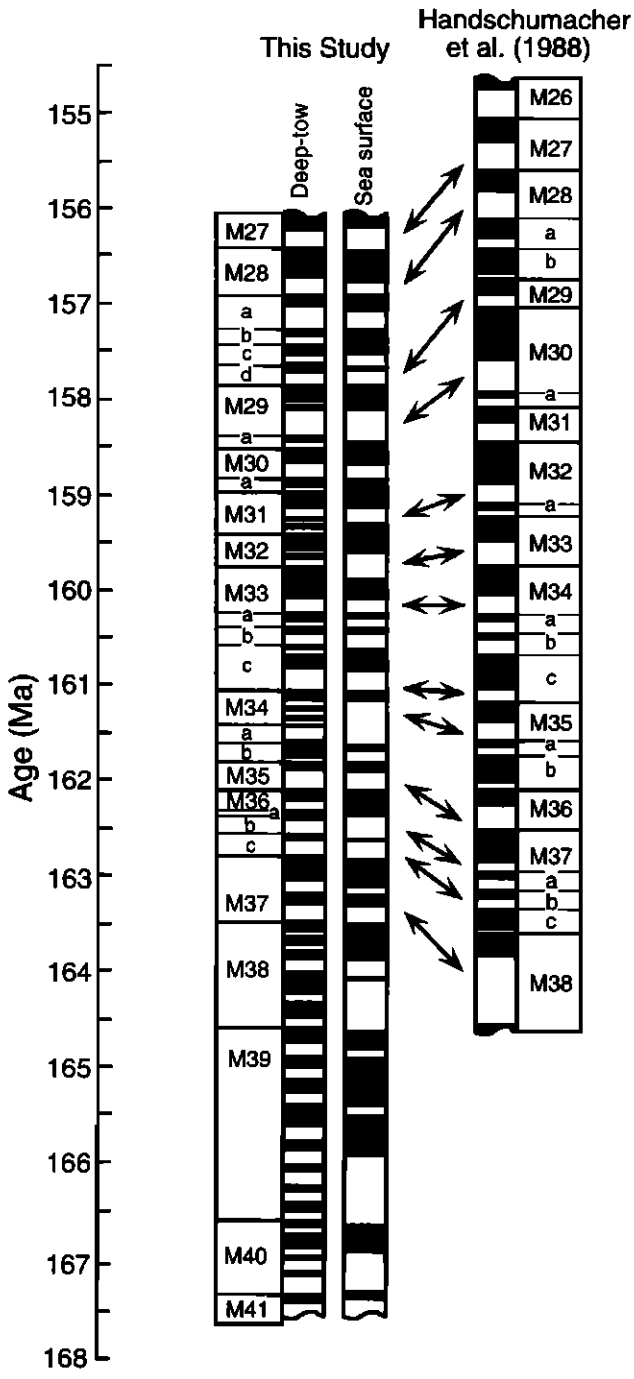

Figure 9. (left) Magnetic polarity model from this study compared with that of *Handschumacher et al.* [1988] (right). Age is shown on the vertical scale. Black areas in columns represent normal magnetic polarity whereas white areas denote reversed polarity. Two timescales are shown from this study; one was derived from the deep-tow magnetic model, and the other was derived from the deep-tow data upward continued to the sea surface. Note that our anomaly numbers differ by 1 from those in *Handschumacher et al.* [1988], that is, M30 from their GPTS is M29 in our model. *Handschumacher et al.* [1988] redefined M29, but others [*Lancelot et al.*, 1990; *Nakanishi et al.*, 1992] recognize their M30 as the original M29 defined by *Cande et al.* [1978]. The arrows show correlations between timescales. Boundary ages are given in Tables 1 and 2.

have acted globally because the same amplitude envelope is seen in other oceans [e.g., *Hayes and Rabinowitz*, 1975]. One example is a global change in the magnetic minerals emplaced at spreading ridges, like that postulated to explain the difference between Cretaceous and late Cenozoic basalt magnetizations [*Johnson and Pariso*, 1993]. We see two problems with this explanation: (1) our low deep-tow model magnetizations greatly differ from Hole 801C data and (2) the geomagnetic field was also behaving unusually at the same time as implied by large numbers of anomalies. Occam's Razor suggests that we make the simplest assumption, that the geomagnetic field was the cause of the low intensities and the rapid variations. Unfortunately, estimates of Jurassic field strength are few because samples of Jurassic oceanic crust are rare [*Johnson and Pariso*, 1993], so we have no independent data to support this conclusion.

By any approach our data imply that Jurassic geomagnetic field behavior was unusual. If we interpret the anomalies as polarity reversals, our model implies that the field had an extraordinarily low intensity and high reversal rate of ~12 per m.y. (Figure 10), ~70% and 20% higher than the late Miocene and the period between M25 and M26, respectively, periods in the accepted GPTS with the greatest reversal rates. If we conclude instead that the older, short-wavelength anomalies are paleointensity fluctuations, the reversal rate is decreased to about Miocene level (which is rapid, nevertheless), but our data suggest that these paleointensity changes dominated the field variations as recorded in the oceanic crust. Since magnetostratigraphic results imply that many of the larger anomalies on the younger ends of the profiles are polarity reversals, this would imply that our data show the transition from a geomagnetic field whose variations were dominated by intensity changes to one dominated by reversals. Examining the data closely, we find that at ~450 km (M36-M37) the anomaly variations shift from regular, smaller anomalies to larger, less regular anomalies (Figures 4 and 5), so the change may have been abrupt. Even if we assume that the true magnetic field behavior was some combination of these two end-members, the conclusion must be that the field was in a low-intensity, rapid-reversal state.

Finally, if the sea surface model is the better polarity record, does this imply that deep-tow data are not worth the extra effort to acquire them? Our data clearly provide a high-quality, high-signal-to-noise record of the oldest magnetic lineations known. They show short-wavelength anomalies that correlate well and apparently reflect geomagnetic field behavior. With additional deep-tow data, presumably, more details of geomagnetic history could be deciphered. Unfortunately, any magnetic anomaly data are nonunique, and ultimately, verification whether a wiggle is a wobble or a flip must come from magnetostratigraphic confirmation.

8. Conclusions

We constructed a GPTS based on two deep-tow magnetic anomaly profiles from the Pigafetta Basin. As a whole, the two profiles, separated by 65-110 km, show excellent correlation of anomalies from line to line. On the basis of extrapolation of the spreading rate determined from nearby isochrons M24-M28, the profiles cover ~11 Ma from M27 to a chron we designated M41, which occurred at ~167.5 Ma. The

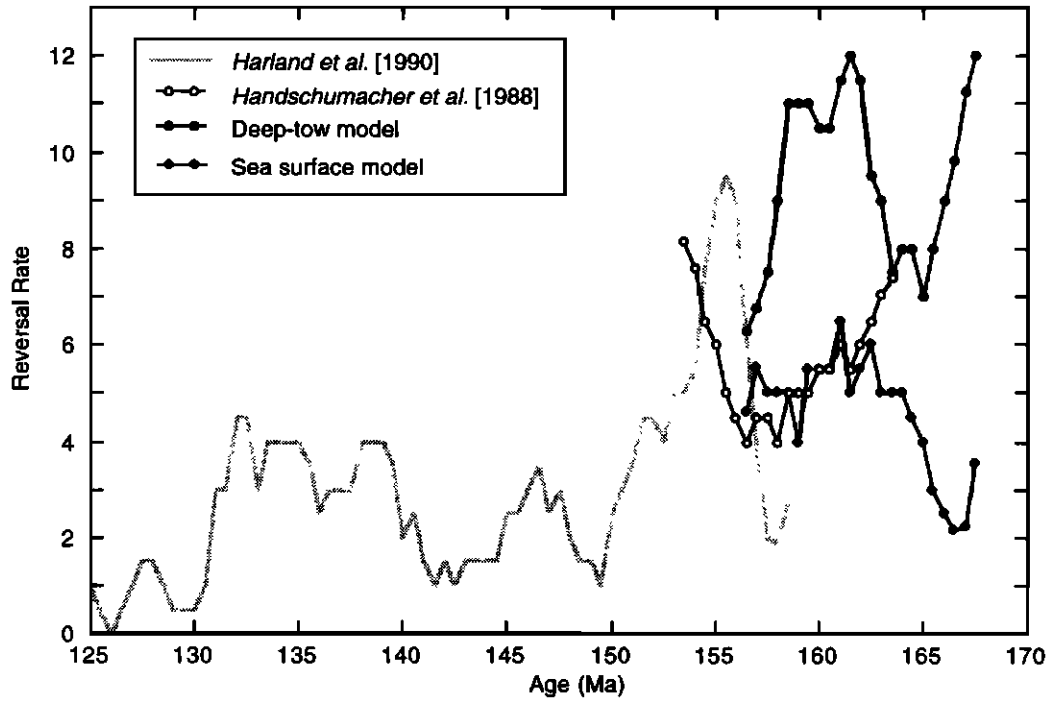

Figure 10. Late Jurassic-Early Cretaceous magnetic polarity reversal rate versus age for the GPTS calculated in this study, *Handschumacher et al.* [1988], and *Harland et al.* [1990]. The upper and lower heavy lines at the right with the solid circles and solid diamonds correspond to our deep-tow and sea surface models, respectively. The heavy line at the right with stipple beneath is the curve calculated from the *Harland et al.* [1990] GPTS. The dotted line at right with the open circles is from the *Handschumacher et al.* [1988] GPTS. Reversal rate values were calculated at 1 m.y. intervals with a 2 m.y. window. The spike at 155 Ma in the Harland et al. GPTS occurs because of the many short chrons between anomalies M24 and M26. The deep-tow model implies an extremely high reversal rate, but the sea surface polarity model is consistent with the elevated but not unusual reversal rate for Late Jurassic time from the *Handschumacher et al.* [1988] and *Harland et al.* [1990] GPTS.

resulting reversal record is dependent on our interpretation of smaller anomalies at the old ends of the profiles. These oldest anomalies have wavelengths that imply polarity interval durations of 150-300 kyr. If we assume that they are caused by reversals, the GPTS implies an extremely high reversal rate, as much as 12 m.y.$^{-1}$ These smaller anomalies are superimposed on longer-wavelength anomalies, which cannot be easily modeled with the observation datum close to the magnetic source (i.e., at deep-tow depths). Consequently, we constructed a derivative model based on the magnetic profiles upward continued to the sea surface. This model is similar to previous models of these anomalies by *Handschumacher et al.* [1988]. It contains fewer short duration chrons, owing to smoothing of the anomalies by upward continuation, and consequently a lesser reversal rate. This model implies that the short-wavelength anomalies are largely paleointensity fluctuations superimposed on longer-polarity chrons, which are represented by the longer-wavelength anomalies. Because of the similarity of the short-wavelength anomaly periods to postulated long-term paleointensity variations and the fact that the sea surface model is more readily reconcilable with magnetization intensities from basalts cored at nearby ODP Site 801, we suggest that the GPTS derived from the sea surface model is a more conservative representation of polarity history. Both deep-tow profiles show an increase in anomaly amplitude by a factor of ~5 going forward in time, a trend that continues to M21 time, a period of ~20 m.y. This trend dictates that the model magnetization intensities also increase with time. We think that a crustal process cause of this magnetization increase is implausible, so we postulate that it has a geomagnetic field cause. Magnetostratigraphic studies show that polarity reversals occurred during most of the period represented by our profiles, so we are convinced that many anomalies, especially the younger ones, are actually caused by polarity reversals. This conclusion suggests that our profiles possibly record a transition in geomagnetic field behavior from one in which field fluctuations were dominated by intensity variations to one dominated by polarity reversals.

Appendix

For the reader who wishes to use our anomaly sequence to generate a timescale using a different base GPTS, we give the following instructions and data (Table A1). Taking the anomaly boundary distances given in the table and the boundary ages from a favorite timescale, one makes a linear regression for the slope, which is the spreading rate. The age of chrons in our sequences can be calculated using the composite sequence distances (Tables 1 and 2) and attaching to one distance the age of one of the base GPTS chron

boundaries. We calculated boundary ages for the deep-tow profile models using the expression age (Ma) = 156.41 + (x - 0.0154). The figure 156.41 is the *Harland et al.* [1990] GPTS date for the old boundary of M27r, an easily recognizable anomaly at the young end of our profiles. Our polarity reversal sequence can be adapted to new versions of the GPTS by substituting the age of M27r in the above formula and recalculating the slope of the anomaly versus distance curve from Figure 8 and Table 1. Although the tables give the boundary ages to 0.001, this is the model resolution, not the absolute age accuracy.

Table A1. Polarity Chron Boundary Distance on D/V *Glomar Challenger* Leg 89 Tie Line

Boundary	Distance km	Boundary	Distance km
M23r (o)	49		
M24r (y)	64	M24-1 (y)	74
M24-1 (o)	86	M24r (o)	97
M24Ar (y)	103	M24Ar (o)	124
M24Br (y)	143	M24Br (o)	150
M25r (y)	157	M25r (o)	168
M25An-1 (y)	177	M25An-1 (o)	180
M25An-2 (y)	186	M25An-2 (o)	188
M25Ar (y)	196	M25Ar (o)	199
M26n-1 (y)	209	M26n-1(o)	210
M26n-2 (y)	215	M26n-2 (o)	217
M26n-3 (y)	226	M26n-3 (o)	228
M26r (y)	238	M26r (o)	248
M27r (y)	257	M27r (o)	264
M28r (y)	280	M28r (o)	299
M29r (y)	371	M29r (o)	384

Boundaries are for reversed polarity chrons. (y) designates younger boundary and (o) designates older boundary. Chron nomenclature is from *Harland et al* [1982, 1990]

Acknowledgments. We thank the captain and crew of the R/V *Thomas Washington* for their aid and perseverance in collecting our data, B. Halbert and P. Crampton for assistance with the geophysical instruments at sea, and R. Johnson and the University of Washington Oceanography Technical Services group for constructing the deep-tow magnetometer. We thank T. Burkhart for his efforts digitizing magnetic observatory records. Discussions with D. Handschumacher helped lay the foundation for this project. Constructive reviews by M. Steiner, R. Larson, and associate editor T. Hildenbrand were instrumental in improving this manuscript. This research was supported by NSF grant OCE88-17553.

References

Abrams, L. J., R. L. Larson, T. H. Shipley, and Y. Lancelot, Cretaceous volcanic sequences and Jurassic oceanic crust in the East Mariana and Pigafetta Basins of the western Pacific, in *The Mesozoic Pacific: Geology, Tectonics, and Volcanism. Geophys Monogr Ser* vol. 77, edited by M. S. Pringle et al., pp. 77-101, AGU, Washington, D. C., 1993.

Alt, J. C., C. France-Lanord, P. A. Floyd, P. Castillo, and A. Galy, Low-temperature hydrothermal alteration of Jurassic ocean crust, Site 801, *Proc. Ocean Drill. Prog., Sci. Results, 129*, 415-427, 1992.

Barrett, D. L., and C. E. Keen, Mesozoic magnetic lineations, the magnetic quiet zone, and sea floor spreading in the northwest Atlantic, *J. Geophys. Res., 81*, 4875-4884, 1976.

Blakely, R. J., Geomagnetic reversals and crustal spreading rates during the Miocene, *J. Geophys. Res., 79*, 2979-2985, 1974.

Blakely, R. J., and A. Cox, Evidence for short geomagnetic polarity intervals in the early Cenozoic, *J. Geophys. Res., 77*, 7065-7072, 1972.

Brenner, C., and M. Angell, Data report: Bathymetry of the Pigafetta and East Mariana Basins, *Proc. Ocean Drill. Prog., Sci. Results, 129*, 693, 1992.

Burek, P. J., Magnetic reversals: their application to stratigraphic problems, *Am. Assoc. Petr. Geol. Bull., 54*, 1120-1139, 1970.

Cande, S. C., and D. V. Kent, Constraints imposed by the shape of marine magnetic anomalies on the magnetic source, *J. Geophys. Res., 81*, 4157-4162, 1976.

Cande, S. C., and D. V. Kent, A new geomagnetic polarity time scale for the Late Cretaceous and Cenozoic, *J. Geophys. Res., 97*, 13,917-13,951, 1992a.

Cande, S. C., and D. V. Kent, Ultrahigh resolution marine magnetic anomaly profiles: A record of continuous paleointensity variations?, *J. Geophys. Res., 97*, 15,075-15,083, 1992b.

Cande, S. C., and D. V. Kent, Revised calibration of the geomagnetic polarity timescale for the Late Cretaceous and Cenozoic, *J. Geophys. Res., 100*, 6093-6095, 1995.

Cande, S. C., and J. L. LaBrecque, Behavior of the Earth's paleomagnetic field from small scale marine magnetic anomalies, *Nature, 247*, 26-28, 1974.

Cande, S. C., J. L. LaBrecque, and R. L. Larson, Magnetic anomalies in the Pacific Jurassic Quiet Zone, *Earth Planet. Sci. Lett., 41*, 434-440, 1978.

Channel, J. E. T., E. Erba, M. Nakanishi, and K. Tamaki, Late Jurassic-Early Cretaceous time scales and oceanic magnetic anomaly block models, in *Geochronology, Time Scales, and Global Stratigraphic Correlation, SEPM Spec. Publ.*, vol. 54, pp. 51-63, Soc. for Sediment. Geol., Tulsa, Okla., 1995.

Clement, B. M., and D. V. Kent, Short polarity intervals within the Matuyama transitional field records from hydraulic piston core sites in the North Atlantic, *Earth Planet. Sci. Lett., 81*, 253-264, 1987.

Dyment, J., and J. Arkani-Hamed, Spreading-rate-dependent magnetization of the oceanic lithosphere inferred from the anomalous skewness of marine magnetic anomalies, *Geophys. J. Int., 121*, 789-804, 1995.

Dyment, J., S. C. Cande, and J. Arkani-Hamed, Skewness of marine magnetic anomalies created between 85 and 40 Ma in the Indian Ocean, *J. Geophys. Res., 99*, 24,121-24,134, 1994.

Floyd, P. A., and P. R. Castillo, Geochemistry and petrogenesis of Jurassic ocean crust basalts, Site 801, *Proc. Ocean Drill. Prog., Sci. Results, 129*, 361-388, 1992.

Gradstein, F. M., F. P. Agterberg, J. G. Ogg, J. Hardenbol, P. van Veen, J. Thierry, and Z. Huang, A Mesozoic timescale, *J. Geophys. Res., 99*, 24,051-24,074, 1994.

Gromme, C. S., and R. L. Hay, Geomagnetic polarity epochs: Age and duration of the Olduvai normal polarity event, *Earth Planet. Sci. Lett., 10*, 179-185, 1971.

Guspi, F., Frequency domain reduction of potential field measurements to a horizontal plane, *Geoexploration, 24*, 87-98, 1987.

Handschumacher, D. W., W. W. Sager, T. W. C. Hilde, and D. R. Bracey, Pre-Cretaceous tectonic evolution of the Pacific plate and extension of the geomagnetic polarity reversal timescale with implications for the origin of the Jurassic "Quiet Zone," *Tectonophysics, 155*, 365-380, 1988.

Harland, W. B., A. V. Cox, P. G. Llewellyn, C. A. G. Pickton, A. G. Smith, and R. Walters, *A Geologic Time Scale*, 131 pp., Cambridge Univ. Press, New York, 1982.

Harland, W. B., R. L. Armstrong, A. V. Cox, L. E. Craig, A. G. Smith, and D. G. Smith, *A Geologic Time Scale 1989*, 265 pp., Cambridge Univ. Press, New York, 1990.

Hayes, D. E., and P. D. Rabinowitz, Mesozoic magnetic lineations and the magnetic quiet zone off northwest Africa, *Earth Planet. Sci. Lett., 28*, 105-115, 1975.

Heirtzler, J. R., and D. E. Hayes, Magnetic boundaries in the North Atlantic Ocean, *Science, 157*, 185-187, 1967.

Heirtzler, J. R., G. O. Dickson, E. M. Herron, W. C. Pitman III, and X.

LePichon, Marine magnetic anomalies, geomagnetic field reversals, and motions of the ocean floor and continents, *J. Geophys Res.*, *73*, 2119-2136, 1968.

Helsley, C E., and M. B. Steiner, Evidence for long intervals of normal polarity during the Cretaceous period, *Earth Planet Sci. Lett.*, *5*, 325-332, 1969.

Hildebrand, J A., and R. L. Parker, Paleomagnetism of Cretaceous Pacific seamounts revisited, *J Geophys Res.*, *92*, 12,695-12,712, 1987.

Ito, H., Y. Nogi, and R L Larson, Magnetic structures of seamounts in the western Pacific Ocean deduced from Leg 144 downhole magnetometer logs, *Proc. Ocean Drill. Prog., Sci. Results*, *144*, 631-638, 1995

Johnson, H. P., and R. T Merrill, A direct test of the Vine-Matthews hypothesis, *Earth Planet Sci Lett.*, *40*, 263-269, 1978

Johnson, H P., and J. E. Pariso, Variations in oceanic crustal magnetization Systematic changes in the last 160 million years, *J. Geophys Res.*, *98*, 435-445, 1993

Juárez, M. T., M. L. Osete, G. Melendez, and W Lowrie, Oxfordian magnetostratigraphy in the Iberian Range, *Geophys. Res Lett.*, *22*, 2889-2892, 1995.

Kent, D V., and F M. Gradstein, A Cretaceous and Jurassic chronology, *Geol. Soc. Am. Bull.*, *96*, 1419-1427, 1985.

Kovacs, L. C., and P. R. Vogt, Depth-to-magnetic source analysis of the Arctic Ocean region, *Tectonophysics*, *89*, 255-294, 1982

LaBrecque, J. L., D. V. Kent, and S. C. Cande, Revised magnetic polarity timescale for Late Cretaceous and Cenozoic time, *Geology*, *5*, 330-335, 1977.

Lancelot, Y., R. L. Larson, and Shipboard Scientific Party, *Proceedings of the Ocean Drilling Program, Initial Reports*, vol. 129, Ocean Drill. Progr., College Station, Tex., 1990.

Larson, R. L., Latest pulse of the Earth: Evidence for a Mid-Cretaceous super plume, *Geology*, *19*, 963-966, 1991.

Larson, R L., and C G. Chase, Late Mesozoic evolution of the western Pacific Ocean, *Geol. Soc Am. Bull.*, *83*, 3627-3644, 1972

Larson, R L., and T W C. Hilde, A revised time scale of magnetic reversals for the Early Cretaceous and Late Jurassic, *J. Geophys. Res.*, *80*, 2586-2594, 1975.

Larson, R. L., and W C. Pitman III, World-wide correlation of Mesozoic magnetic anomalies, and its implications, *Geol. Soc. Am. Bull.*, *83*, 3645-3662, 1972

Larson, R. L., and W. W. Sager, Skewness of magnetic anomalies M0 to M29 in the northwestern Pacific, *Proc Ocean Drill. Prog., Sci. Res.*, *129*, 471-481, 1992

Larson, R. L., and S. O. Schlanger, Geological evolution of the Nauru Basin and regional implications, *Initial Rep Deep Sea Drill Proj.*, *61*, 841-862, 1981.

Larson, R. L., M. B. Steiner, E. Erba, and Y. Lancelot, Paleolatitudes and tectonic reconstructions of the oldest portion of the Pacific plate: A comparative study, *Proc. Ocean Drill. Prog., Sci. Results*, *129*, 615-631, 1992.

Ludden, J., Radiometric age determinations for basement from Sites 765 and 766, Argo Abyssal Plain and northwestern Australia, *Proc. Ocean Drill. Prog., Sci. Results*, *123*, 557-559, 1992.

Marzocchi, W., Missing reversals in the geomagnetic polarity timescale Their influence on the analysis and in constraining the process that generates geomagnetic reversals, *J. Geophys. Res.*, *102*, 5157-5171, 1997.

Meynadier, L., J -P. Valet, R. Weeks, N. J. Shackleton, and V. L Hagee, Relative geomagnetic intensity of the field during the last 140 ka, *Earth Planet. Sci. Lett.*, *114*, 39-57, 1994.

Nakanishi, M., K. Tamaki, and K. Kobayashi, Mesozoic magnetic anomaly lineations and seafloor spreading history of the northwestern Pacific, *J. Geophys. Res.*, *94*, 15,437-15,462, 1989.

Nakanishi, M., K. Tamaki, and K. Kobayashi, Magnetic anomaly lineations from Late Jurassic to Early Cretaceous in the west central Pacific Ocean, *Geophys. J Int.*, *109*, 701-719, 1992.

Ogg, J. G., Magnetic polarity time scale of the Phanerozoic, in *Rock Physics and Phase Relations: A Handbook of Physical Constants, AGU Ref. Shelf*, vol. 3, edited by T. J. Ahrens, pp. 240-270, AGU, Washington, D.C., 1995.

Ogg, J. G., and J. Gutowski, Oxfordian magnetic polarity time scale, in *Proceedings of the 4th International Congress on Jurassic Stratigraphy and Geology, Geo. Res. Forum* vols. 1-2, edited by A. C. Riccardi, pp. 406-414, Trans-Tec Publ. Ltd., Zurich, Switzerland, 1996.

Onwumechilli, A., Geomagnetic variations in the equatorial zone, in *Physics of Geomagnetic Phenomena*, vol. 1, edited by S. Matsushita and W. H. Campbell, pp. 426-507, Academic Press, San Diego, 1967.

Ozima, M., I. Kaneoka, K. Saito, M. Honda, M. Yanagisawa, and Y. Takigami, Summary of geochronological studies of submarine rocks from the western Pacific Ocean, in *Geodynamics of the Western Pacific-Indonesian Region, Geodyn. Ser.*, vol. 11, edited by T. W. C. Hilde and S. Uyeda, pp. 137-142, AGU, Washington, D.C., 1983.

Parker, R. L., Coherence of signals from magnetometers on parallel paths, *J. Geophys. Res.*, *102*, 5111-5117, 1997.

Press, W. H., B. P. Flannery, S. A Teukolsky, and W. T Vetterling, *Numerical Recipes*, 818 pp., Cambridge Univ. Press, New York, 1986

Pringle, M. S., Radiometric ages of basaltic basement recovered at Sites 800, 801, and 802, Leg 129, western Pacific Ocean, *Proc Ocean Drill. Prog., Sci Results*, *129*, 389-404, 1992.

Rea, D K., and R. J. Blakely, Short-wavelength magnetic anomalies in a region of rapid seafloor spreading, *Nature*, *255*, 126-128, 1975

Sager, W W., Seamount age estimates from paleomagnetism and their implications for the history of volcanism on the Pacific plate, in *Geology and Offshore Mineral Resources of the Central Pacific Basin, Earth Science Series*, vol 14, edited by B. Keating and B Bolton, pp 21-37, Circum-Pacific Council for Energy and Mineral Resources, Springer-Verlag, New York, 1992

Sager, W W., L. G. Fullerton, R T Buffler, and D W Handschumacher, Argo Abyssal Plain magnetic lineations revisited, implications for the onset of seafloor spreading and tectonic history of the Eastern Indian Ocean, *Proc. Ocean Drill Prog., Sci. Results*, *123*, 659-669, 1992.

Schlanger, S. O., H. C Jenkyns, and I. Premoli-Silva, Volcanism and vertical tectonics in the Pacific basin related to global transgressions, *Earth Planet. Sci. Lett.*, *52*, 435-449, 1981.

Schouten, H., and K. McCamy, Filtering marine magnetic anomalies, *J Geophys Res.*, *77*, 7089-7099, 1972.

Schouten, J. A., A fundamental analysis of magnetic anomalies over oceanic ridges, *Mar. Geophys. Res.*, *1*, 111-144, 1971.

Smith, G M., The magnetic structure of the marine basement, *Rev. Aquat. Sci.*, *2*, 205-227, 1990.

Smith, W. H. F., H. Staudigel, A B Watts, and M S. Pringle, The Magellan Seamounts: Early Cretaceous record of the south Pacific isotopic and thermal anomaly, *J. Geophys. Res.*, *94*, 10,501-10,523, 1989

Spector, A., and F. S. Grant, Statistical models for interpreting aeromagnetic data, *Geophysics*, *35*, 293-302, 1970

Steiner, M. B., and J G Ogg, Early and Middle Jurassic magnetic polarity time scale, in *2nd International Symposium on Jurassic Stratigraphy*, vol 2, edited by R. B. Rocha and A. F Soares, pp. 1097-1111, Cent. de Estratigrafia e Paleobiol da Univ Nova de Lisboa, Lisbon, 1988.

Steiner, M. B., and B. P. Wallick, Jurassic to Paleocene paleolatitudes of the Pacific plate derived from the paleomagnetism of the sedimentary sequences at sites 800, 801, and 802, *Proc Ocean Drill. Prog., Sci. Results*, *129*, 431-446, 1992

Steiner, M. B., J G Ogg, G. Melendez, and L. Sequeiros, Jurassic magnetostratigraphy, 2. Middle-Late Oxfordian of Aguilon, Iberian cordillera, northern Spain, *Earth Planet. Sci. Lett.*, *76*, 151-166, 1985

Talwani, M., and J. R. Heirtzler, Computation of magnetic anomalies caused by two-dimensional structures of arbitrary shape, in *Computers in the Mineral Industries*, edited by G. A Parks, pp. 464-480, Stanford Univ Press, Stanford, Calif., 1964.

Tarduno, J. A., W. V. Sliter, L. Kroenke, M Leckie, H. Mayer, J J. Mahoney, R. Musgrave, M. Storey, and E. L. Winterer, Rapid formation of Ontong Java Plateau by Aptian mantle plume volcanism, *Science*, *254*, 399-403, 1991

Taylor, P T., and D. Greenewalt, Geophysical transitions across the northwest Atlantic magnetic quiet zone, *Earth Planet. Sci. Lett.*, *29*, 435-446, 1976.

Vine, F J., and D. H. Matthews, Magnetic anomalies over oceanic ridges, *Nature*, *199*, 947-949, 1963.

Wallick, B. P., and M B. Steiner, Paleomagnetic and rock magnetic

properties of Jurassic Quiet Zone basalts, Hole 801C, *Proc Ocean Drill. Prog., Sci. Results, 129*, 455-470, 1992.

Wilson, D S., and R. N Hey, The Galapagos axial magnetic anomaly: evidence for the Emperor event within the Brunhes and for a two-layer magnetic source, *Geophys Res. Lett., 8*, 1051-1054, 1981.

Winterer, E. L., J. H. Natland, R. J. van Waasbergen, R. A. Duncan, M. K. McNutt, C. J Wolfe, I. Premoli-Silva, W. W. Sager, and W. V. Sliter, Cretaceous guyots in the northwest Pacific: An overview of their geology and geophysics, in *The Mesozoic Pacific: Geology, Tectonics, and Volcanism, Geophys. Monogr. Ser.* vol. 77, edited by M S Pringle et al., pp. 307-334, AGU, Washington, D. C., 1993

H. P. Johnson, School of Oceanography, University of Washington, Seattle, WA 98195-7940. (email: johnson@ocean.washington.edu)

W. W. Sager, Department of Oceanography, Texas A&M University, College Station, TX 77843-3146. (email, wsager@ocean.tamu.edu)

M. A. Tivey, Department of Geology and Geophysics, Woods Hole Oceanographic Institution, Woods Hole, MA, 02543. (email: mtivey@whoi..edu)

C. J. Weiss, Department of Geology and Geophysics, Texas A&M University, College Station, TX 77843-3114. (email: cjw9199@geopsun tamu.edu)

(Received June 26, 1997; revised October 15, 1997; accepted November 18, 1997.)